Structure and Dielectric Properties of Barium−Strontium Niobate Thin Films Grown on MgO(110) and MgO(001) Single-Crystal Substrates

© *D.V. Stryukov, Ya.Yu. Matyash, A.V. Pavlenko*

Southern Scientific Center, Russian Academy of Sciences,
Rostov-on-Don, Russia

E-mail: strdl@mail.ru

$Sr_{0.6}Ba_{0.4}Nb_2O_6$ thin films of $\sim 550\,nm$ thickness with a preliminarily deposited conductive $SrRuO_3$ layer of $\sim 150\,nm$ thickness were grown on MgO(110) and MgO(001) substrates by RF-cathode sputtering in an oxygen atmosphere. X-ray diffraction studies have shown that the obtained films have no unit cell strain, while for barium−strontium niobate film on an MgO(110) substrate it has been found for the first time that the [001] polar axis lies in the interface plane with the substrate. It is shown that the films differ significantly in surface morphology, dielectric and ferroelectric properties measured in the out-of-plane direction.

Keywords: thin films, barium−strontium niobate, SBN, MgO(110) substrate.

1. Introduction

$(Sr,Ba)Nb_2O_6$ barium−strontium niobate is a uniaxial ferroelectric (its polarization is directed along the c axis) known since 1960 [1]. $(Sr,Ba)Nb_2O_6$ crystallizes with the structure of tetragonal tungsten bronze with $P4bm$ space group in the Sr concentration range from 25 to 75% [2], with the Curie temperature T_C of the ferroelectric crystal decreasing from approximately 220°C (at a Sr concentration of 25%) to approximately 60°C (at a Sr concentration of 75%) [3,4]. The framework of the $(Sr,Ba)Nb_2O_6$ structure consists of NbO_6 octahedra arranged in the form of pentagons, providing three types of interstitial positions: triangular positions remain free, and the quadrangular and pentagonal positions are partially occupied (five out of six possible) by Sr and Ba atoms and partially vacant (one out of six possible) [5]. Due to this fact the local composition of $(Sr,Ba)Nb_2O_6$ can vary from cell to cell; as a result, many barium−strontium niobates are ferroelectric relaxors with a highly diffuse phase transition. Ferroelectric relaxors are widely used in capacitors and actuators; in addition, $(Sr,Ba)Nb_2O_6$ demonstrates high values of pyroelectric coefficient and linear electro-optical coefficient [2,4,6,7], which also makes it a promising material for optoelectronic devices and pyroelectric detectors.

The ever-growing need to reduce the size of microelectronics components and integrated optical systems makes the study of materials in the form of thin films extremely popular, in particular, $(Sr,Ba)Nb_2O_6$ [8,9]. Using thin films of $(Sr,Ba)Nb_2O_6$, the possibility to develop electro-optical modulators [10,11], pyroelectric elements [12,13], and phase shifters is already shown [14]. However, despite the existing developments, the issue remains relevant regarding the establishment of the influence of size effects, defects and strains of unit cell on the ferroelectric, dielectric, and nonlinear optical properties of $(Sr,Ba)Nb_2O_6$ thin films. The unit cell strains of thin films strongly depend on the production method and on the choice of the substrate for the deposition, and it is also necessary to take into account the fact that epitaxial films of $(Sr,Ba)Nb_2O_6$ exhibit spontaneous formation of orientation domains with the rotation of the axes relative to the substrate axes by 0, 18.4, and 31° (Figure 1) [15,16]. To date, thin films of $(Sr,Ba)Nb_2O_6$ have already been successfully produced by various sputtering techniques: pulsed laser deposition [14,15], sol-gel [17,18], RF sputtering [16,19], molecular-beam epitaxy [20], metalorganic chemical vapor deposition [21] and precipitation from an aqueous solution [22,23].

However, for this purpose semiconductor (Si) and dielectric (MgO, Al_2O_3 and $SrTiO_3$) wafers exclusively with the (001) orientation were used as substrates. The use of other orientations substrates can make it possible to obtain both significant strains of the unit cells and other than [001] unit cell orientations of $(Sr,Ba)Nb_2O_6$ films, and films without orientation domains. This can make it possible to both control the properties of the material and enhance some of them, for example, for $KNbO_3$ an increased electro-optical coefficient was found for a film with the (111) orientation compared to the (001) orientation [24]. At the same time, thin-film structures having their polar axis located in the interface plane are quite rarely studied. However, such structures can potentially be used, for example, in optical devices where a controlled domain structure with vertical domain walls is required, as well as in hyperfine films,
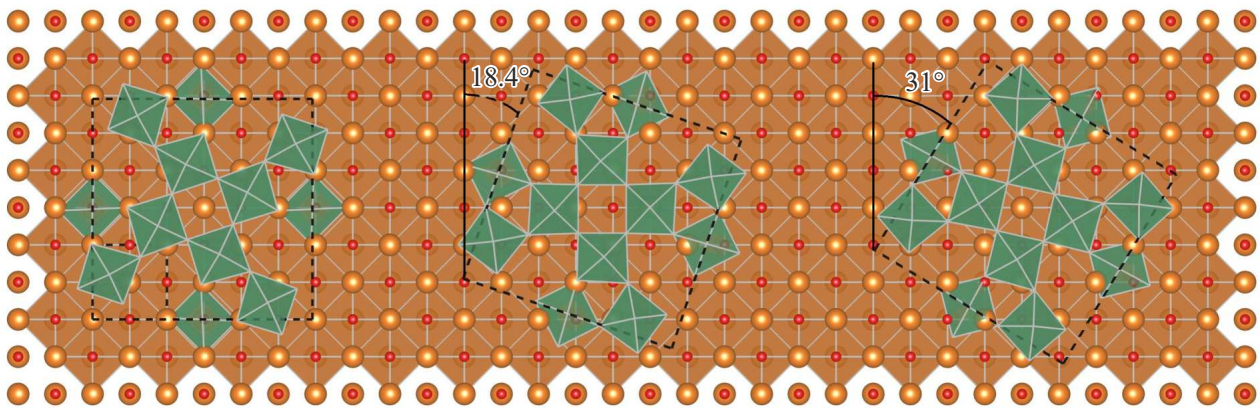
Figure 1. Schematic representation of the mutual orientation of MgO unit cells and orientation domains of $(Sr, Ba)Nb_2O_6$: their crystallographic axes are rotated by 0, 18.4, and $31°$ relative to each other.

where the in-plane polarization can make it possible to avoid the effect of increasing depolarization field. In this study, $Sr_{0.6}Ba_{0.4}Nb_2O_6/SrRuO_3$ heterostructures were produced on MgO (110) and MgO(001) substrates, and the effect of substrate orientation on their phase composition, structural features, surface morphology and properties (dielectric and ferroelectric) was investigated.

2. Materials and methods

$Sr_{0.6}Ba_{0.4}Nb_2O_6$ (SBN) and $SrRuO_3$ (SRO) films with a thickness of ~ 550 and $\sim 150\,nm$, respectively, were deposited using high-frequency cathode sputtering on two specialized units. First, a conductive SRO layer was deposited onto a MgO substrate with (001) or (110) orientation, and then a SBN layer was deposited on top of it. The oxygen pressure for deposition of both films was $67\,Pa$, the substrate temperature before the discharge turning on was $400°C$. After deposition of the SRO layer, the sample was cooled in an oxygen atmosphere to a temperature of $\sim 30°C$, then the sample was moved to the second chamber for the deposition of the SBN layer. Thus, two heterostructures were produced: SBN60/SRO/MgO(001) (SBN-1) and SBN60/SRO/MgO(110) (SBN-2).

The crystal structure of the samples was studied by X-ray diffraction method using a RIKOR multifunctional X-ray difractometer with Bragg-Brentano focusing, a goniometer with a step of up to $0.001°$ (Crystal Logic Inc.), and a BSV21-Cu X-ray tube („Svetlana-Roentgen" JSC), a scintillation detector (ITC„Radikon" LLC).

To study the surface morphology of a two-layer heterostructure, a „Ntegra Academia" atomic force microscope (NT-MDT, Russia) was used. The topography of the samples was obtained in the semi-contact mode using a NS15/50 silicon cantilever (NT-MDT, Russia). The scanning rate of a $10 \times 10\,\mu m^2$ surface relief fragment with a resolution of 400 points per line was $1\,Hz$. The obtained

scans were processed and analyzed in the Image Analysis software.

The real (ε') and imaginary (ε'') parts of the complex dielectric constant at the frequencies f of the measuring electric field in a range of $10 \ldots 250\,kHz$ with an amplitude of $40\,mV$ were measured at temperatures of $-185 \ldots 200°C$ using an Agilent 4980A LCR meter and a Linkam THMS600 temperature stage. Dynamic dielectric hysteresis loops of $P(E)$ at a frequency of $1\,kHz$ were measured using a TF Analyzer 2000 and a MST4000A analytical probe station.

3. Experimental results and discussion

Using the X-ray diffraction method, $\theta - 2\theta$ X-ray patterns were recorded for SBN-1 and SBN-2 heterostructures (Figure 2), where only reflections related to the film and substrate layers were detected. No traces of impurity phases, such as $SrNb_2O_6$ and $BaNb_2O_6$, were found. The SBN layer on the MgO(001) substrate is epitaxial with the polar axis [001] oriented perpendicular to the substrate plane (c-oriented) and there are the formation of orientation domains where in-plane axes are rotated by $\pm 18.4°$ relative to the axes of the substrate, similarly to [19]. However, the SBN layer on the MgO(110) substrate is a polycrystalline textured layer with a predominant orientation of the [400] axis perpendicular to the substrate plane (a-oriented), thus, the polar axis [001] lies in-plane. From the data obtained, the lattice constants of the SBN were determined: $c = 3.959\,Å$, $a = 12.41\,Å$ for the SBN-1 heterostructure and $a = 12.46\,Å$ for the SBN-2 heterostructure. Due to the low intensity of the X-ray lines in the SBN-2, it was not possible to reliably determine the c parameter. Thus, the unit cell of the SBN thin film on substrates of both orientations, (001) and (110), has almost no in-plane strains compared to the unit cell of a bulk material ($a_{bulk} = 12.46\,Å$ and $c_{bulk} = 3.936$ [5]).

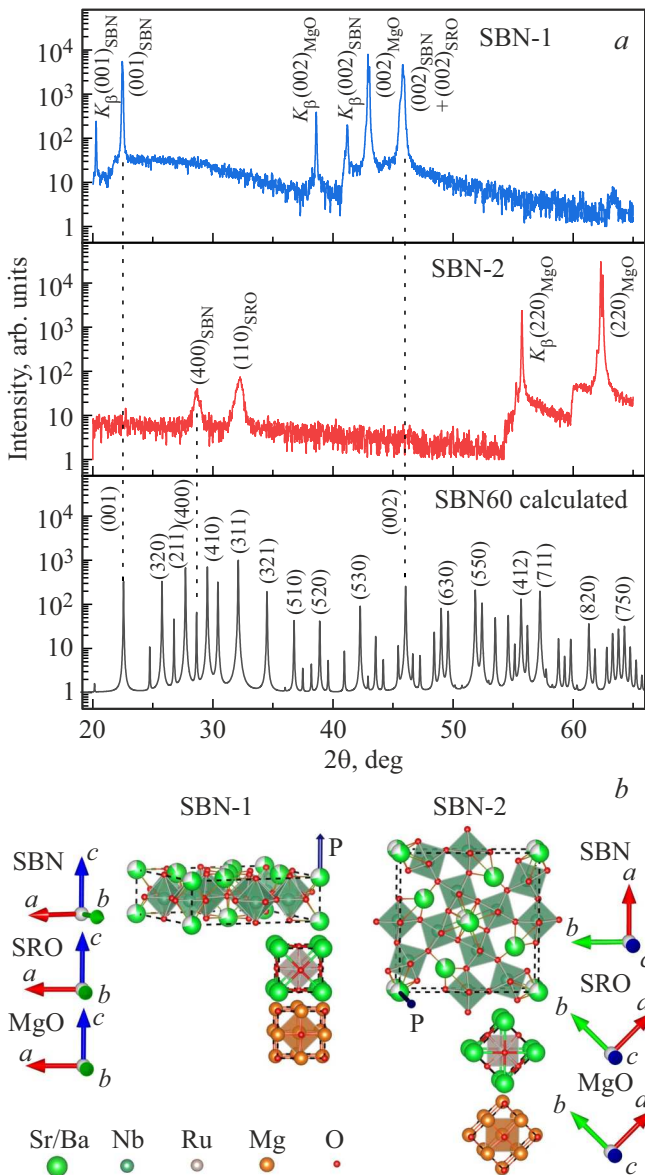**Figure 2.** *a*) $\theta-2\theta$ X-ray patterns of SBN-1 (top) and SBN-2 (in the center) heterostructures, and also for comparison the theoretically calculated X-ray pattern for polycrystal SBN60 (bottom). *b*) Model of mutual orientation of film and substrate unit cells for SBN-1 and SBN-2, respectively.

Figure 3 shows the surface relief images of SBN-1 and SBN-2. It can be seen that the topography of the films differs significantly depending on the orientation of the MgO substrate. The surface of the SBN-2 heterostructure (Figure 3, *d*) is represented by growth blocks of different shapes and sizes: from small ($\sim 50-75$ nm) crystallites with mainly oval shape and smooth boundaries to large (> 200 nm) trapezoidal inclusions with rounded edges. At the same time, the film does not contain cavities and other surface defects (Figure 3, *b*).

In the case of SBN-1 (Figure 3, *a*), large pores with a size of $\sim 500-550$ nm (average depth of the pores is

$\sim 60-70$ nm) are observed, no individual blocks with clear boundaries are recorded, and the relief is represented by large flat areas (Figure 3, *c*), at the junctions of which small depressions are formed (with an average depth of $\sim 10-15$ nm). Histograms of the height distribution over the surface are shown in Figure 3, *a* and 3, *b*. For the SBN-2 heterostructure, the histogram is symmetrical, without any features, and the root-mean-square roughness (RMSR) value for it from the surface fragment of $100 \mu m^2$ was ~ 13.9 nm. The histogram of surface height distribution for the SBN-1 heterostructure has a noticeable asymmetry in the negative part of the distribution associated with the presence of pores and small depressions on the surface, which also led to an increased RMSR value. The RMSR value for SBN-1 was 16.1 nm (table) and is comparable to the value for SBN-2. It is also worth noting that despite the presence of depressions, the SBN-1 heterostructure is characterized by a smoother topography compared to SBN-2, which can be seen on scans with a size of $3 \times 3 \mu m^2$ (Figure 3, *c* and 3, *d*). The height difference across the film surface when deposited on the (001)MgO substrate is 1.6 times less than that on the (110)MgO substrate.

The fact that the polar axis in the SBN-1 film is directed normally to the substrate and in the SBN-2 it lies in the plane of film-to-substrate interface has clearly manifested when studying the dielectric and ferroelectric properties of the samples in the out-of-plane direction (Figure 4−6). To implement it, capacitor structures were formed: the lower electrode was an SRO layer, and the upper electrode was an Ag/Pd alloy deposited by magnetron sputtering in an argon atmosphere by an Emitech SC7620 unit through a mask with hole diameter of $90-100 \mu m$.

As can be seen from Figure 4, the typical ferro-electrics response was clearly observed only for SBN-1: at $E \sim 160$ kV/cm an elongated loop was recorded (maximum P_{max} and residual P_R polarization and coercive field E_C were $32.4 \mu C/cm^2$, $10.3 \mu C/cm^2$ and 29.7 kV/cm, respectively). For the SBN-2 at E in the range of $0-160$ kV/cm, in turn, hysteresis-free almost linear $P(E)$ dependencies were recorded with $P_{max} = 1.9 \mu C/cm^2$, which is indicative of the absence of signs of polarization switching in the sample in the out-of-plane direction. A significant difference in properties, due to the fact that SBN are uniaxial ferroelectrics [2], has manifested when analyzing the $\varepsilon'(E)$ dependencies of the samples (Figure 5). At $E = 0$ kV/cm, in the SBN-2 the relative dielectric constant was 130, and in the SBN-1 it was 1150. When an electric field with an amplitude of $E = 160$ kV/cm is applied, the dielectric constant of the SBN-1 first increases (from 1150 to 1425), in the vicinity of E_C it passes through its maximum, and then decreases down to 750, and in the SBN-2 it remains almost unchanged.

As can be seen from Figure 6, in the temperature range from $-190°C$ to $200°C$ values of ε' and ε'' for the SBN-1 always exceed those for the SBN-2, at the same time, in contrast to the SBN61 single crystal [25],
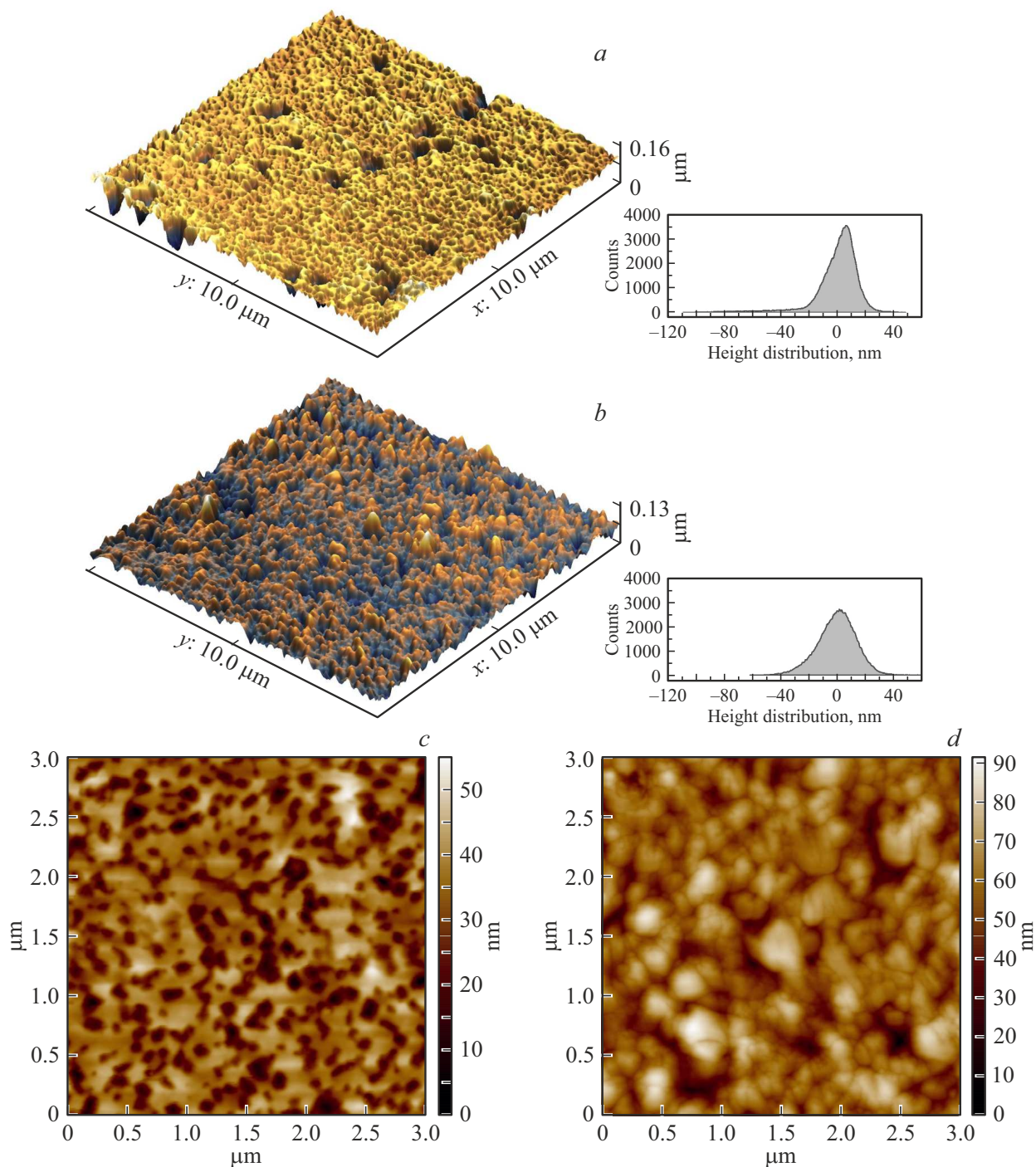
Figure 3. Topography of $10 \times 10 \, \mu m^2$ and histograms of surface height distribution (a, b), as well as precision topography of $3 \times 3 \, \mu m^2$ (c, d), for SBN-1 and SBN-2, respectively.

Structural and dielectric characteristics of SBN-1 and SBN-2 heterostructures

Heterostructure	Orientation	a, Å	c, Å	RMSR, nm	ε'_{RT}	P_R, μC/cm^2	P_{max}, μC/cm^2	E_C, kV/cm
SBN-1	(001)	12.41	3.959	13.9	1150	10.3	32.4	29.7
SBN-2	(110)	12.46	−	16.1	130	0.16	1.9	~ 10

N o t e : ε'_{RT} is real part of the dielectric constant at room temperature.
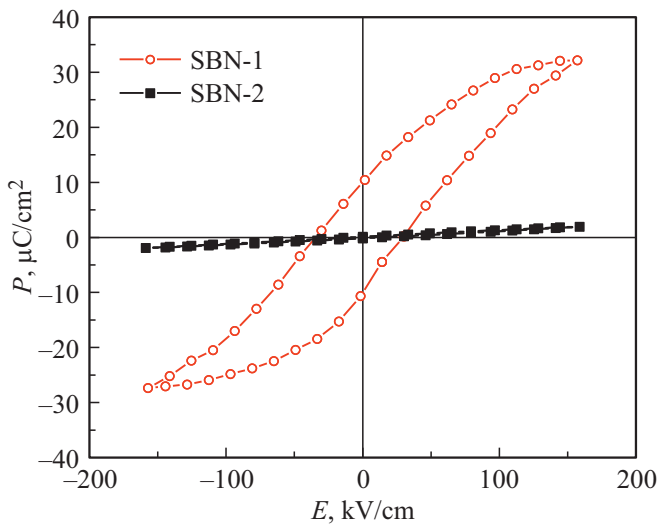

Figure 4. $P(E)$ dependence for SBN-1 and SBN-2 heterostructures at a temperature of 24°C, at a frequency of 1 kHz.
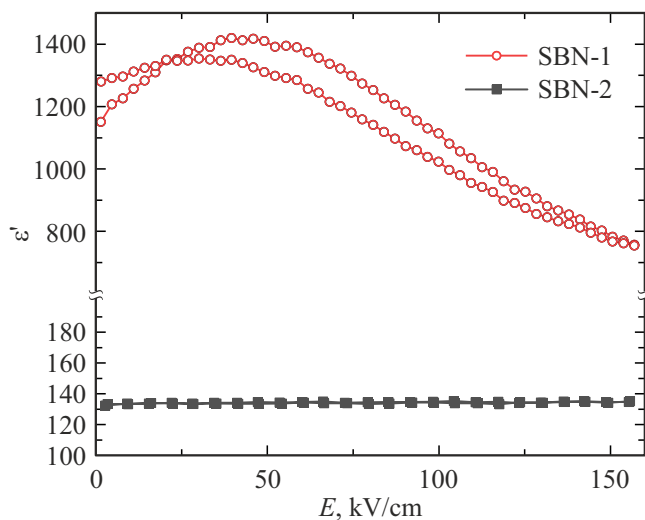

Figure 5. $\varepsilon'(E)$ dependencies at a temperature of 24°C, at a frequency of 10 kHz for SBN-1 and SBN-2 heterostructures. Sweep period of the external triangular field is 1 Hz.

a dispersion of dielectric constants is recorded in both films at all temperatures. The increase in ε' and ε'' in both samples at $T > 160$°C is associated with an increase in the electrical conductivity of the films at these temperatures and an increase in the contribution from the

polarization of Maxwell−Wagner type. When analyzing the $\varepsilon'(T, f)$ and $\varepsilon''(T, f)$ dependencies in the region of the diffuse paraelectric → ferroelectric phase transformation, it is clear that when in the SBN-1 a typical behavior of ferroelectric relaxor is observed (maximum at $\varepsilon'(T)$ with growing f decreases in value and shifts to the region of high temperatures from 115°C to 131°C), in the SBN-2 only an anomaly is recorded at $T \approx -10$°C (inset in Figure 6, b). Despite the fact that no pronounced anomalies are observed in the SBN-1 film at $T \approx -10$°C, it turned out that the temperature hysteresis disappears at this temperature in $\varepsilon'(T)$ and $\varepsilon''(T)$ dependencies (Figure 6, c).

4. Conclusion

For the first time, an undoped $Sr_{0.6}Ba_{0.4}Nb_2O_6$ film with (400) orientation was produced on a SRO/MgO(110) substrate, where the polarization lies in the plane of film-to-substrate interface. For comparison, under identical conditions, a $Sr_{0.6}Ba_{0.4}Nb_2O_6$ film was produced on an SRO/MgO(001) substrate with its polar axis is normal to the surface of the substrate. At the same time, both films were impurity-free, had almost no unit cell strain, and were characterized by comparable surface roughness (less than 16.5 nm, with a thickness of 550 nm), however their morphology was significantly different.

A significant difference in the properties of the samples was clearly manifested when analyzing the $P(E)$ and $\varepsilon'(E)$ dependencies in the direction normal to the substrate surface, where the film on MgO(001) exhibits a ferroelectric polarization loop of an elongated shape and a good controllability along ε', but the film on MgO(110) demonstrates hysteresis-free, almost linear dependence of polarization on the external field and a lack of controllability by ε'. In turn, in the $\varepsilon'(T, f)$ and $\varepsilon''(T, f)$ dependencies for the film on MgO(110), a feature was discovered at ~ -10°C, which coincides with the temperature at which the temperature hysteresis disappears in the film on MgO(001).

Thus, the results obtained suggest that using the high-frequency cathode deposition method it is possible to change the mutual orientation of the crystallographic axes of the $Sr_{0.6}Ba_{0.4}Nb_2O_6$ film and the MgO substrate by choosing the orientation of the substrate and thereby it is possible to control the direction of polarization, which is manifested in a significant change in dielectric and
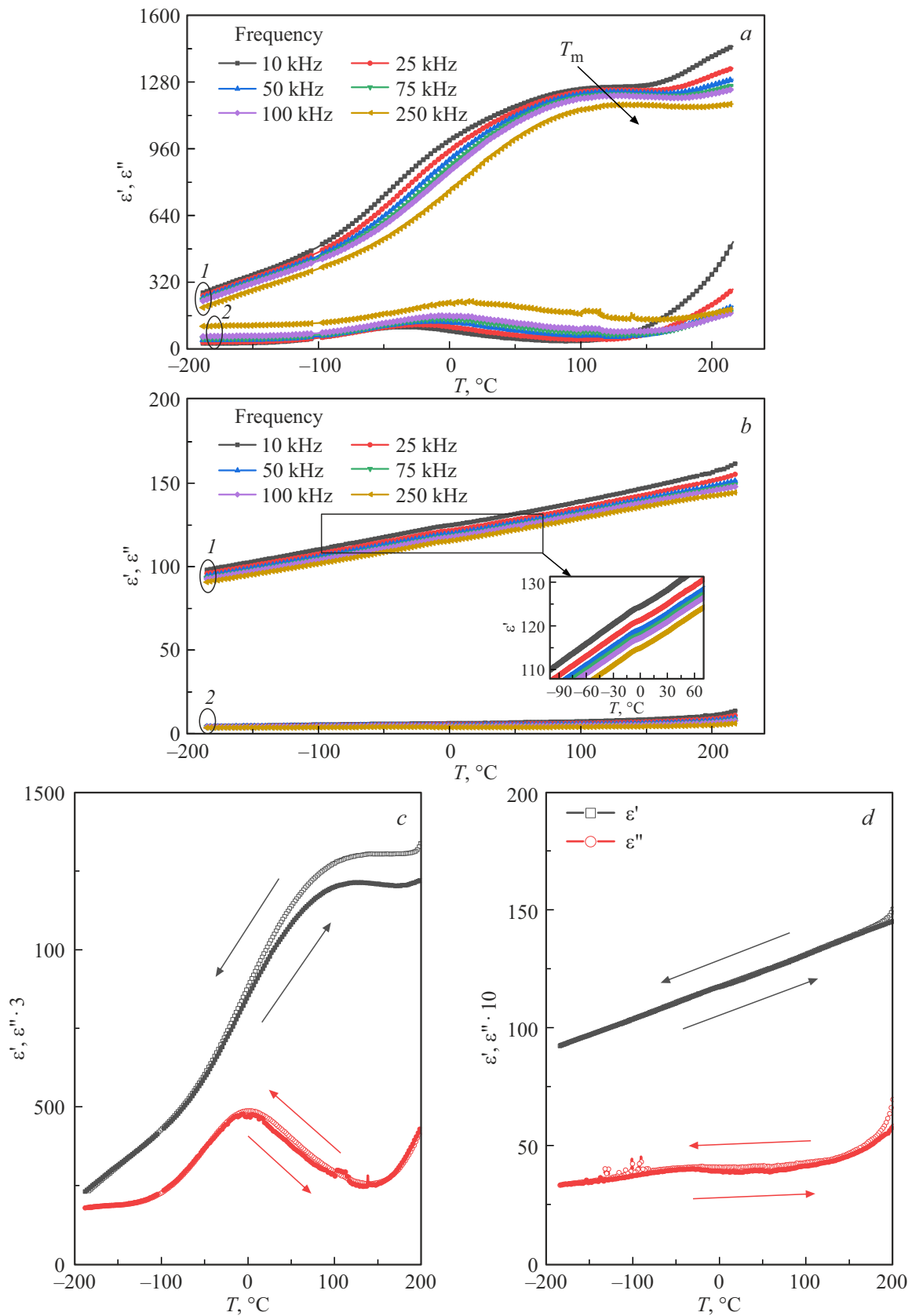
Figure 6. $\varepsilon'(T, f)$ (curves *1*) and $\varepsilon''(T, f)$ (curves *2*) dependencies for SBN-1 (*a*) and SBN-2 (*b*) heterostructures recorded in the heating mode, the inset shows a zoomed-in temperature range of $-100-70°C$. The $\varepsilon'(T, f)$ and $\varepsilon''(T, f)$ dependencies at a frequency of 100 kHz in heating and cooling modes (temperature changes are shown by arrows) of SBN-1 (*c*) and SBN-2 (*d*) heterostructures.

ferroelectric properties of the film in the direction normal to the substrate surface.

Funding

Conflict of interest

The authors declare that they have no conflict of interest.

References

[1] M.H. Francombe. Acta Cristallogr. **13**, 131 (1960).

[2] Yu.S. Kuzminov, Segnetoelektricheskie kristally dlya upravleniya lazernym izlucheniem, Nauka, M., (1982), 400 s. (in Russian).

[3] A.A. Ballman, H. Brown. J. Cryst. Growth **1**, *5*, 311 (1967).

[4] N.S. VanDamme, A.E. Sutherland, L. Jones, K. Bridger, S.R. Winzer. J. Am. Ceram. Soc. **74**, *8*, 1785 (1991).

[5] S. Podlozhenov, H.A. Graetsch, J. Schneider, M. Ulex, M. Wöhlecke, K. Betzler. Acta Crystallogr. B **62**, 960 (2006).

[6] S. Sakamoto, T. Yazaki. Appl. Phys. Lett. **22**, 429 (1973).

[7] V.V. Shvartsman, D.C. Lupascu. J. Am. Ceram. Soc. **95**, *1*, 1 (2012).

[8] E.G. Kostsov. Ferroelectrics **314**, 169 (2005).

[9] M. Cuniot-Ponsard. Strontium Barium Niobate Thin Films for Dielectric and Electro-Optic Applications. In Ferroelectrics-Material Aspects / Ed. M. Lallart. InTech, Rijeka, Croatia (2011) P. 497−518.

[10] S. Gupta, A. Paliwal, V. Gupta, M. Tomar. Opt. Laser Technol. **122**, 105880 (2020).

[11] S. Gupta, A. Paliwal, V. Gupta, M. Tomar. Opt. Laser Technol. **137**, 106816 (2021).

[12] S. Ivanov, E.G. Kostsov. IEEE Sens. J. **20**, *16*, 9011 (2020).

[13] V.N. V'yukhin, S.D. Ivanov. Optoelectron. Instrum. Data Proc. **54**, 502 (2018).

[14] S.E. Moon, M.H. Kwak, Y.-T. Kim, H.-C. Ryu, S.-J. Lee, K.-Y. Kang. J. Korean Phys. Soc. **46**, *1*, 273 (2005).

[15] P.R. Willmott, R. Herger, B.D. Patterson, R. Windiks. Phys. Rev. B **71**, 144114 (2005).

[16] A.V. Pavlenko, D.V. Stryukov, L.I. Ivleva, A.P. Kovtun, K.M. Zhidel, P.A. Lykov, FTT **63**, *2*, 250 (2021). (in Russian).

[17] J. Koo, J.H. Jang, B.-S. Bae. J. Am. Ceram. Soc. **84**, *1*, 193 (2001).

[18] Y. Xu, C.J. Chen, R. Xu, J.D. Mackenzie. Phys. Rev. B **44**, 35 (1991).

[19] M. Cuniot-Ponsard, J.M. Desvignes, B. Ea-Kim, E. Leroy. J. Appl. Phys. **93**, 1718 (2003).

[20] I.M. Beskin, S. Kwon, A.B. Posadas, M.J. Kim, A.A. Demkov. Adv. Photon. Res. **2**, *10*, 2100111 (2021).

[21] M.J. Nystrom, B.W. Wessels, W.P. Lin, G.K. Wong, D.A. Neumayer, T.J. Marks. Appl. Phys. Lett. **66**, 1726 (1995).

[22] V.H. Pedersen, A.B. Blichfeld, K. Bakken, D. Chernyshov, T. Grande, M.-A. Einarsrud. Cryst. Growth Des. **22**, *10*, 5912 (2022).

[23] M.K. Lee, R.S. Feigelson. J. Cryst. Growth **180**, 220 (1997).

[24] T.M. Graettinger, S.H. Rou, M.S. Ameen, O. Auciello, A.I. Kingon. Appl. Phys. Lett. **58**, 1964 (1991).

[25] A.V. Pavlenko, L.I. Ivleva, D.V. Stryukov, A.P. Kovtun, A.S. Anokhin, P.A. Lykov, FTT **61**, *2*, 376 (2019). (in Russian).

Translated by Y.Alekseev